D24

N82 23442

Size distribution of Oceanic air bubbles entrained in sea-water by wave-breaking*

François Resch

Université de Toulon, Château Saint Michel, 83130 La Garde, France

François Avellan

Ecole Polytechnique Fédérale de Lauzanne, CH1015, Switzerland

Abstract

The determination of the size of oceanic air bubbles produced by whitecaps and wave-breaking is of great importance for predicting the production of liquid aerosols at the sea surface. These liquid aerosols are at the origin of most of the particulate materials exchanged between the ocean and the atmosphere. As no standard measurement techniques are presently available, a prototype has been especially designed and built using an optical technique. This technique is based on the principle of light scattering at an angle of ninety degrees from the incident light beam. The output voltage is a direct function of the bubble diameter. Calibration of the probe has been carried out within a range of 300 μm to 1.2 mm. Bubbles are produced by wave-breaking in a large air-sea interaction simulating facility. Experimental results are given in the form of size spectrum.

Introduction

The production of marine aerosols, responsible for the transfer of large quantities (10^{10} tons fo salt per year) of materials from the ocean to the atmosphere, is governed by the bursting ting if air bubbles at the air-sea interface. These air bubbles are produced in bulk sea water by wave-breaking. After a variable life-span in water, the bubbles move up to the surface, burst and produce either jet drops or film drops or, most commonly, both simultaneously. The production of water droplets depends on the size of the generating air bubble. Consequently we have to determine the size-distribution, the concentration and the injection depths of this air bubble population in order to be able to predict the production of marine aerosols under varying wind conditions. This is of fundamental importance for our physico-chemical environment.

The physical mechanisms of bubble and drop production

When the wind speed is high enough, the waves become unstable and break. This leads to the presence of whitecaps at the sea surface and the penetration of air bubbles into bulk sea water. Although the mechanism by which these bubbles are introduced in water is not yet clear, it is thought that their presence might result principally from the three following processes : i) the formation of a roller at the wave crest engulfs a certain amount of air which is broken up in the water. This leads to the presence of larger bubbles close to the sea surface.

ii) the wave crest produces a plunging-like liquid jet which penetrates the sea water and leads to the production of bubbles of various sizes at various depths.

iii) the two-phase flow roller of the breaking wave slides down by gravity along the wave slope. This gravitational action combined with the horizontal shear stresses produced at the base of the roller introduces a large number of air bubbles near the throw of the wave, just as in the case of an hydraulic jump[1].

The injected bubbles are carried downwards by means of a water flow in one or a combination of the above patterns.

During their life-span in water (see figure 1), these air bubbles will be exposed to dynamic forces (drift currents, orbital movements), mass exchanges (growth or dissolution) and chemical reactions (collection of surfactants at their interface)[2].

Owing to buoyancy forces, these bubbles return to the sea surface and break. This breaking leads to the formation of two families of droplets, the so-called "film drops" and "jet drops"[3, 4].

*Research done at the "Institut de Mécanique Statistique de la Turbulence". Laboratoire associé au CNRS, Université d'Aix-Marseille, 13003 Marseille, France.

Film drops are micronic in size. Their number is an increasing function of the generating bubble diameter. Jet drops are of a size approximate to 1/10 of the diameter of the generating bubble and their number is decreasing function of the size of the generating bubble. To date little is yet known about these two functions due to the large number of parameters involved.

It is to be noted that the bursting phenomenon is strongly dependent on the chemical composition of the interfacial microlayer.

To summarize, the production of marine liquid aerosols appears to result from a "cascade" or "chain" process[5] as schematically shown on Figure 2.

From the above description it appears evident that the determination of bubble characteristics such as size, injection depth and concentration, is of a particular importance.

The measurement of bubble size

To date few investigators have tried to use various techniques to measure oceanic air bubble size. An acoustic technique was used by Medwin[6], a trapping technique by Blanchard and Woodcock[7] and by Kolovayev[8], and a photographic method was used by Johnson and Cooke[9]. The results of these measurements have been carefully reviewed and compared by Wu[10]. The net result, however, is that more systematic measurements must be obtained by means of a reliable and proven technique.

After reviewing the various techniques available for detecting bubble size within the range 50 μm to 5 mm, a local optical probe was selected.[13]

1 - The principle of operation

The principle of operation of the optical probe is based on the measurement of the light flux scattered at an angle of ninety degrees from the incident light beam when a bubble is passing through the "sensing" volume. In the diameter range considered, the output signal, a direct function of the scattered flux, is proportional to the square of the bubble diameter. A simple calibration of the probe permits one to know the coefficient of proportionality.

2 - Characteristics of the probe

The optical probe is schematically represented on Figure 3. The light source is made of a 2 mW He - Ne laser tube. The sensing volume. determined by the slit D1 and the diaphragm D2 approximately cylindrical in shape with a 500 μm diameter and a 300 μm height (see Figure 4). The light intensity should be uniformly distributed in this sensing volume. This is achieved by the presence of the two above-mentioned diaphragms D1 and D2.

It is important to mention that it is not the real bubble diameter d which is detected, but only the image of these diaphragms through the lenses in the bubble. This leads to an apparent diameter kd of the bubble, where k is independent of d and (here) of the order of 1/20. This enables one to measure bubbles with a diameter larger than the "sensing" volume.

The laser source, the optical system, the photoamplifier and its associated electronics are gathered in a parallelepipedic waterproof stainless steel case of 5 cm x 10 cm x 30 cm (see Figure 4). A more detailed description of the probe is given by Avellan[11].

3 - Calibration of the probe

As mentioned above, calibration of the probe is necessary in order to convert the output signal voltage into bubble diameter. For this calibration, bubbles of a given and uniform diameter are produced by means of capillary glass-tubes in a unit especially built for this purpose (see Figure 5).

Special care was given so that the bubble completely crossed the "sensing" volume. A few thousand bubbles were so produced, their number carefully recorded and the total volume of air measured with a calibrated glass tube. It was then possible to relate the output voltage to bubble diameter. This was done for four different bubble sizes and, as expected, the output voltage is directly proportional to the square of the bubble diameter (see Figure 6).

Experimental results

1 - Data recording conditions and anticipated errors

Measurements were digitally recorded on magnetic discs and tapes through an analog to

digital converter combined with a mini-computer. In order to record only the presence of bubbles passing through the sensing volume of the probe, an hardware voltage amplitude threshold system was designed.

Side effect errors are possible when a bubble is only partially detected by the sensing volume. This error is an increasing function of the ratio of the bubble volume (based on the diameter kd) to the "sensing"volume . In a first approximation this error was neglected (the maximum value of kd being $\approx \frac{1}{20} \times 500 = 25$ µm is to be compared with the 300 µm/500 µm dimensions of the sensing volume)[10]. A more complete statistical derivation has been developed by Avellan [11]

The error due the simultaneous passage of more than one bubble in the detecting volume V has also been disregarded. The concentration is so small that the probability of finding more than one bubble at the same time in the volume V is very low.

2 - Experimental conditions

Experiments were carried out in the large air-sea interaction facility of the "Institut de Mécanique Statistique de la Turbulence" (I. M. S. T., Marseille, France)[12]. Breaking waves were produced by both wind blowing (at 14m/s) and a wave generator. The probe was completely immersed in the water to a depth of few centimeters below the throw of the wave. Data were recorded during a three hour period. Approximately 500 bubbles were detected.

3 - Bubble size distribution

Voltage histogram and bubble size distribution are shown in Figure 7 and 8 respectively. They are normalized by the exact total number of bubbles detected, 517, and by the voltage window width, 156 mv. On the bubble size spectrum, cinfidence intervals have been reported. On the voltage histogram, larger bubbles, corresponding to values of voltage larger than 8 volts, were not taken into account as the photomultiplier gain was purposely limited.

Discussion and Conclusions

These preliminary results show that such an optical probe can be used with success to determine the size spectra of oceanic air bubbles entrained in sea-water by wave-breaking.

The first obvious observation is that very large confidence intervals exist in the data plot. This is due to the overly small detecting volume for a two-phase flow configuration with a very small concentration of bubbles. If it looks advisable to limit, even to reduce, the recording time, it is then necessary to increase the detecting volume widely. With such a configuration, a factor of 1000 times larger for this volume, i. e. of 10 on the linear sizes would be suitable. This would allow ones not only to decrease the duration of the experiment and to limit the statistical uncertainties but would also drastically decrease the side effect error. In return, the coincidence effect could be increased, but could be easily taken into account during data processing.

It would also seem necessary to improve the resolution of the probe towards the smaller diameters, e. g. less than 200 µm. This is presently being done by replacing the hardware voltage threshold system by a software one and by increasing the sensitivity of the photoamplifier. The software data acquisition control also allows one to record the time intervals between bubble appearance in the "sensing volume" which subsequently gives more information one the two-phase flow configuration.

Thanks to this first set of experimental results presented above, new additional experiments have been performed with the benefit of such improvements as on the probe characteristics and the data treatment. They were performed in the same simulating facility applying various wind conditions at various depths. They are presently under processing.

Acknowledgments

The authors wish to acknowledge the contribution of the research and technical staff of the I. M. S. T. as well as the financial support given by the Centre National de la Recherche Scientifique and the Centre National pour l'exploitation des oceans (grant n°80/2196).

References

1. Resch F. J., Leutheusser H. J. and Alemu S. Bubbly two-phase flow in hydraulic jumps, Journal of the Hydraulics Division, A. S. C. E., 100, No HYI, Proc. Paper 10297, Jan., pp. 137-149. 1974.

2. Blanchard D. C. and Syzdek L. D., Concentration of bacteria in jet drops from bursting bubbles, J. Geophys. Res., 77, 5087-5099, 1972.

3. MacIntyre F., The top Millimiter of the ocean, Scientific American, 230, May 1974.
4. Blanchard D. C., The electrification of the atmosphere by particle from bubbles in the sea, Progress in Oceanography, 1, pp. 73-202. 1963.
5. Resch F. J., Echanges particulaires air-mer (au niveau de l'interface), Proceedings de l'Ecole Européenne d'Eté, Cahiers Jacques Fauchère. Université de Paris VI. 1981.
6. Medwin H., In situ accoustic measurements of bubble populations in coastal ocean waters, J. Geophys. Res., 75, 599-611. 1970.
7. Blanchard D. C. and Woodcock A. H., Bubble formation and modification in the sea and its meteorological sigificance, Tellus, 9, No2, pp. 145-158. 1957.
8. Kolovayev D. A., Investigation of the concentration and statistical size distribution of wind-produced bubbles in the near-surface ocean, Oceanology, Engl. Transl., 15, 659-661. 1976.
9. Johnson B. D. and Cooke R. C., Bubble populations and spectra in coastal waters : a photographic appraoch, J. Geophys. Res., 84, 3761-3765. 1979.
10. Wu J., Bubble populations and Spectra in near-surface ocean : summary and Review of Field Measurements. Journal of Geophys. Res., Vol 86, No C1, pp. 457-463. Jan. 1981.
11. Avellan F., Caractéristiques diphasiques des échanges particulaires à l'interface air-mer : étude météorologique. Thèse de Docteur-Ingénieur, I. M. S. T., Université d'Aix-Marseille.
12. Coantic M., Ramamonjiarisca F., Mestayer P., Resch F. and Favre A., Wind water tunnel simulation of small-scale ocean-atmosphere interactions, J. of Géophys. Res., Vol 86, No C7, pp. 6607-6626. July 1981.
13. Resch F., Measurement techniques in the two-phase flow region of the air-sea interface layer, Proceedings of the dynamic flow conference, 1978.

Figure 1. Schematic representation of the air-sea particulate exchanges.

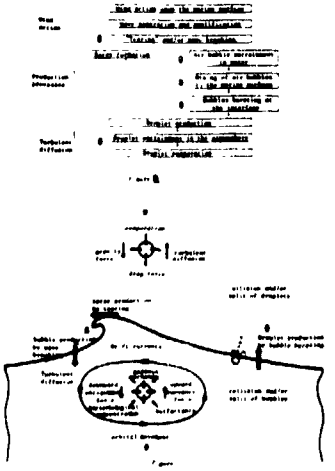

Figure 2. Physical mechanisms for the production of marine liquid aerosols.

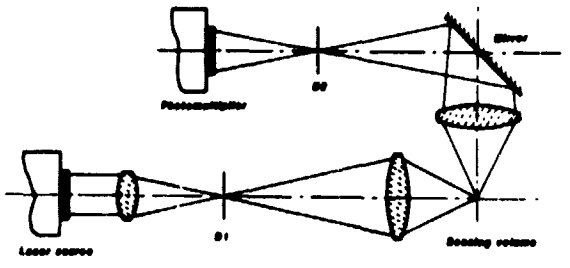

Figure 3. Schematic diagram of the optical part of the probe.

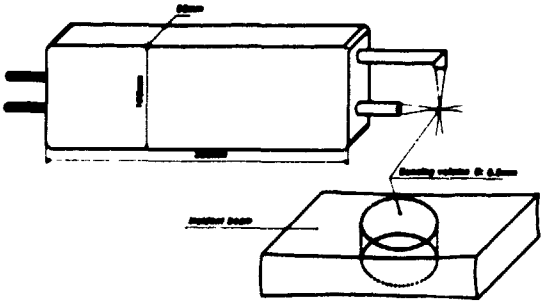

Figure 4. Optical probe with details of the sensing volume.

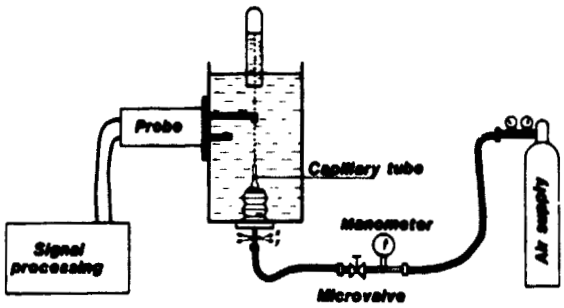

Figure 5. Calibration unit.

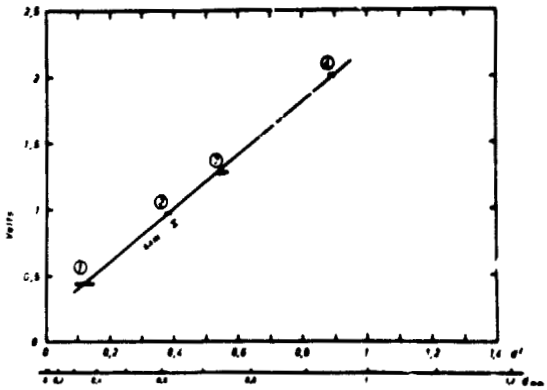

Figure 6. Calibration curve.

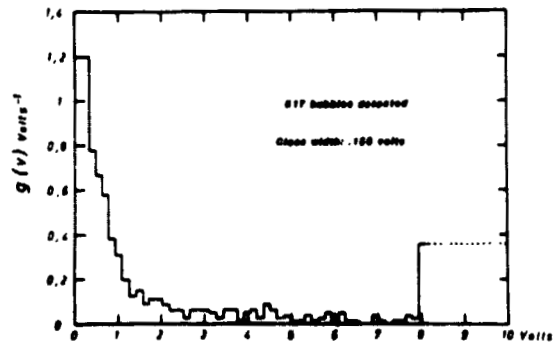

Figure 7. Normalized voltage histogram.

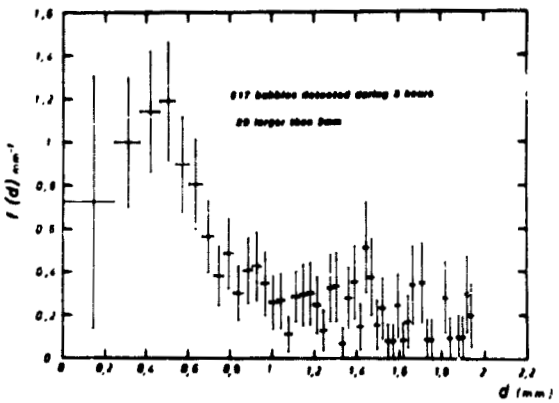

Figure 8. Normalized bubble size spectrum.